Supplementary Material for "Experimental investigation on Rayleigh wave propagation in a locally resonant metamaterial layer resting on an elastic half-space"

Farhad Zeighami,[1,*] Antonio Palermo,[1] Denis Bogomolov,[2] and Alessandro Marzani[1,2]
[1)]*Department of Civil, Chemical, Environmental, and Materials Engineering - DICAM, University of Bologna, Viale del Risorgimento, 2, Bologna 40136, Italy*
[2)]*Advanced Research Center on Electronic Systems "Ercole De Castro" (ARCES), University of Bologna, Viale Carlo Pepoli, 3/2, Bologna 40123, Italy*

S1. PREPARATION OF THE PROTOTYPE PLATE

We manufactured a metamaterial plate with two resonant parts: one side comprised three layers of resonators, while the other side featured five rows of resonators. Each resonant part is composed of several resonators arranged in a regular grid with a spacing of $a = 0.035$ m. Each row of resonators in the experimental prototype plate is constructed by 28 resonant cells (as shown in FIG. 2(b) of the paper) to achieve a total length of $W_{RL} = 0.98$ m.

To create the resonators, holes are drilled into the plate using a CNC machine, and cubic steel masses are press-fitted into these holes. The plate is subsequently cut with high precision from both sides to create the connectors of the resonators. In total, 84 and 140 basic cells are incorporated within the metamaterial plate to form the resonant layers with 3 and 5 rows of resonators, respectively. During the perforation process, careful control is exercised over the cutting parameters, including cutting force, speed, and angle. Such control is essential to minimize the impact of induced residual mechanical stresses on the PVC plate, ensuring its structural integrity and performance.

We emphasize that the proper design of the barrier requires a distance of approximately $5\lambda_h$ from the source to the barrier zone to eliminate near-source effects. Additionally, maintaining a distance of $2\lambda_h$ after the barrier is necessary to minimize wave reflections from the plate boundaries. Preparing and measuring such a test setup involves using a plate with larger dimensions and demands special attention to prevent plate deflection and ensure measurement accuracy. In our proposed test setup, we addressed perturbations generated by the near-source effect and back-reflections from the boundaries during the post-processing phase. As a result, a perfect agreement between experimental results and theoretical/numerical predictions has been achieved.

S2. EXPERIMENTAL DATA ACQUISITION AND SIGNAL PROCESSING

By employing the proposed experimental setup, the objective is to demonstrate and evaluate the performance of the locally resonant wave barriers in attenuating surface waves.

[*)]Corresponding author: farhad.zeighami3@unibo.it

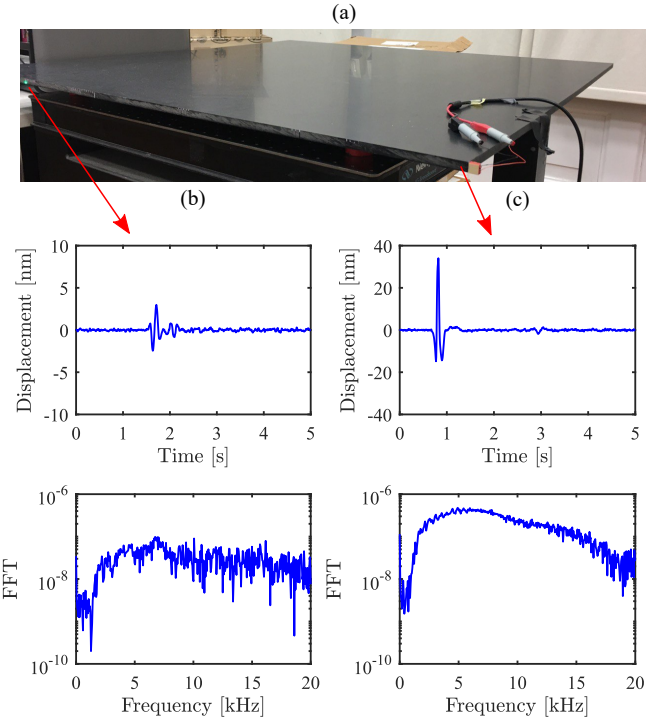

FIG. S1. (a) Test setup for the PVC plate. Signal time trace and its FFT of (b) the furthest point with respect to the source and (c) the closest point.

During our experimental investigation, we used the PVC plate as our reference case study to ensure control over the quality of the transmitted signal and the signal-to-noise ratio. To accomplish this objective, we capture time traces of the output signal from the Scanning Laser Doppler Vibrometer (SLDV). These time traces correspond to the vertical displacement (u_z) at two acquisition points located along the scanning line. One acquisition point is positioned near the piezoelectric transducer, while the other is situated at the end of the acquisition line (refer to FIG. S1(a)).

Subsequently, we perform the Fast Fourier Transform (FFT) on the recorded time traces to analyze the frequency content of the transmitted signal. This enables us to assess the spectral characteristics and frequency components present in the signal, facilitating a thorough investigation of the transmission properties of the PVC plate.

FIG. S1(c) displays the measured output signal from the closest point to the source, along with its corresponding fre-

quency response. The peak displacement observed in the figure is approximately 35 nm, which is one-third of the maximum displacement recorded directly from the surface area of the PZT source, amounting to 115 nm. The frequency content of the output signal demonstrates that it covers the entire frequency range of interest, spanning from 0 to 10 kHz.

FIG. S1(b) illustrates the attenuation of elastic energy associated with surface waves as they propagate toward the far end of the PVC plate. The vertical displacement at the last scanning point, located 0.8 m away from the source, is significantly smaller (approximately one order of magnitude) compared to the previous scanning point. Such an observation indicates the decaying of surface waves as they propagate along the surface of the PVC plate.

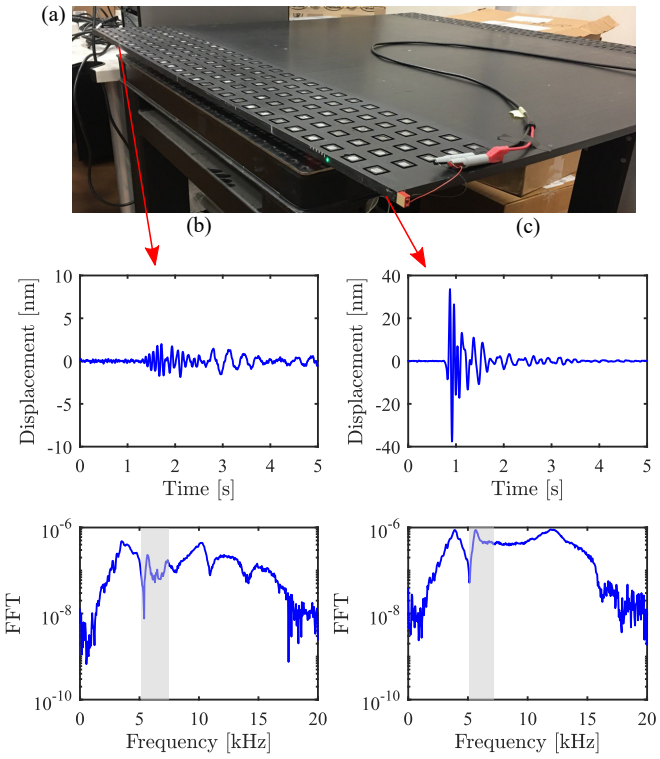

FIG. S2. (a) Test setup for the metamaterial plate with 5 rows of resonant cells. Signal time trace and its FFT of (b) the furthest point with respect to the source and (c) the closest point. The highlighted gray region marks the BG bounds.

We present the corresponding results for the resonant layer equipped with 5 rows of resonators, as depicted in FIG. S2(a). In particular, FIG. S2(c) depicts the measured output signal from the point close to the source, along with its frequency response. The peak displacement observed in the figure falls within the displacement range observed for the reference PVC plate. Interestingly, a notable peak attenuation appears close to the resonant frequency of the resonators (f_r), at 5.2 kHz, at the lower edge of the bandgap region. This attenuation arises from the dynamic coupling between the surface waves and the cluster of sub-wavelength resonators which leads to the scattering of the transmitted signal. Regarding the point farthest from the source, FIG. S2(b) demonstrates a remarkable attenuation of the surface waves. The surface wave attenuation is particularly intensified within the bandgap region, accompanied by a larger peak attenuation around the resonant frequency of the embedded resonators.

S3. EFFECTIVE PARAMETERS OF THE HOMOGENIZED THICK RESONANT LAYER

FIG. S3(a) depicts the effective mass density of the homogenized material, as described in Section IV of the paper. When there is no resonant mass affecting the dynamic inertia of the LRM (i.e., $f_r = 0$), its effective density is equal to the density of the host material, denoted as ρ_h. Furthermore, in the static regime where $f = 0$, the effective mass density $\rho_{eff}(f)$ is equal to the static mass density (ρ_{st}). Conversely, as the frequency tends towards infinity ($f \to \infty$), the effective mass density converges to the density of the host material for all values of f_r.

More importantly, the existence of a bulk bandgap is observed when the effective mass density takes on negative values within the frequency range of $f_{BG,BW} = [5274 - 6472]$ Hz. We note that the width of the bulk bandgap is smaller in magnitude compared to the surface wave bandgap observed in the paper. This is attributed to the presence of a leaky surface mode characterized by a phase velocity higher than the shear velocity of the host material. This leaky surface mode appears in a narrow frequency region above the bulk bandgap, extending the surface wave bandgap[1].

FIGs. S3(b) and (c) present the imaginary and real wavenumbers associated with the evanescent and propagating effective bulk waves of the homogenized locally resonant material, respectively. Both longitudinal and shear waves present hybridized flat branches that asymptotically approach the collective resonant frequency of the resonators (f_r, indicated by the dashed black line). Furthermore, within the frequency range of the bulk bandgap, the effective bulk waves become evanescent waves. This means that the waves no longer propagate through the material but decay exponentially within the bulk region. This behavior is a consequence of the negative effective mass density observed within the bandgap frequency region. We remark that the bandgap of both longitudinal and shear modes occurs within the same frequency region due to the isotropic behavior of the embedded resonators.

S4. NUMERICAL SIMULATIONS AND FINITE ELEMENT MODELS OF SURFACE WAVE PROPAGATION IN THICK LRMS

A. Dispersion relation analysis

We develop numerical models based on the WFEM[3] that combines the Bloch wave theory with the classical finite element method to further validate the experimental and analytical dispersion curves. In this regard, we create three 3D finite element (FE) models of the unit cells using Comsol Multiphysics[2]. These unit cells correspond to the pristine

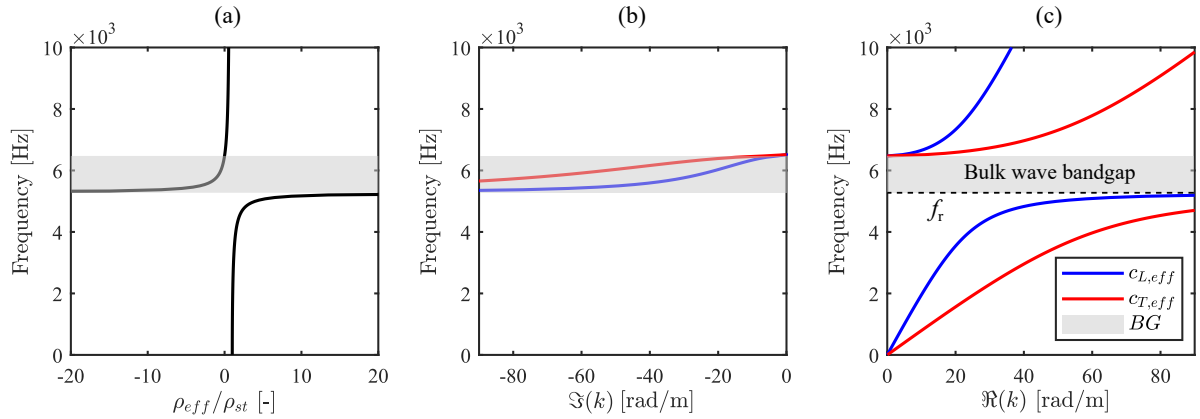

FIG. S3. (a) Effective mass density of LRM. (b) Evanescent and (c) propagating effective bulk waves. The shaded gray area marks the bulk bandgap region.

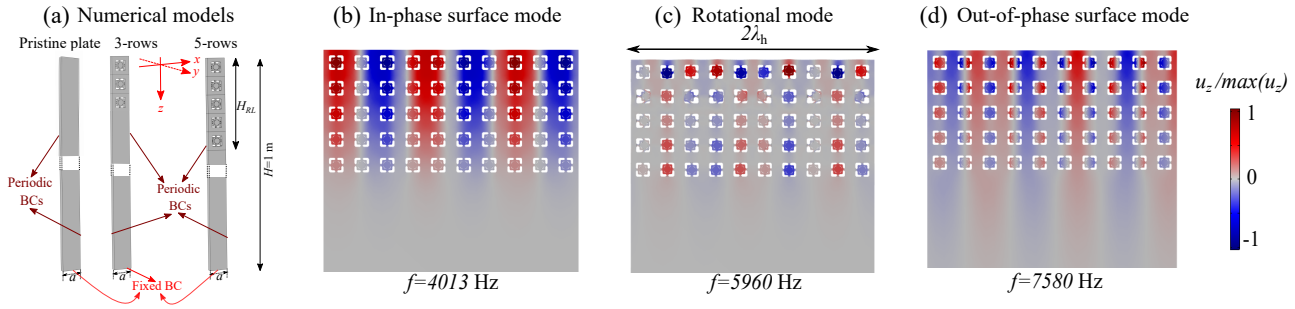

FIG. S4. (a) Schematics of the 3D unit cells of the pristine PVC plate and LRM with 3 and 5 rows of resonators developed in Comsol Multiphysics[2]. The real part of the normalized vertical displacement field of LRM with 5 rows of resonators for $k = 51.29$ [rad/m] corresponding to (b) in-phase surface mode, (c) rotational mode of resonators, and (d) out-of-phase surface mode.

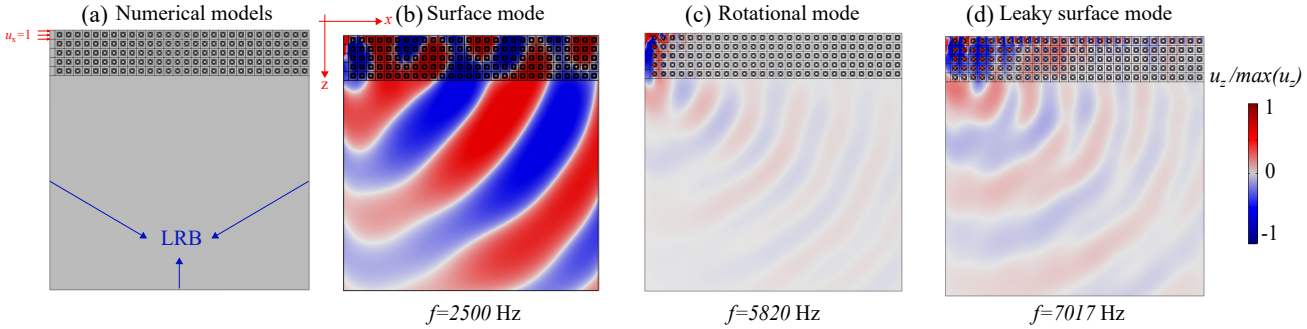

FIG. S5. (a) 2D view of the full 3D numerical model of the metamaterial plate. The normalized vertical displacement field of LRM with 5 rows of resonators obtained from harmonic simulations for (b) surface, (c) rotational, and (d) leaky surface modes.

PVC plate and two LRM configurations with 3 and 5 rows of resonators, respectively (see FIG. S4(a)).

All unit cells have identical dimensions, with a width of a, depth of t, and height of $H = 1$ m (approximately 5 times the reference surface wave wavelength λ_h). The resonators are arranged with a spacing equal to the lattice constant (a) within the material depth to accurately model the resonant layers with a total height of H_{RL}. To ensure proper numerical modeling and avoid undesired motion of the unit cells, we restrict the base displacements of the column cells in all directions. For meshing purposes, we utilize tetrahedral elements with a uniform mesh size of $a/10$ to discretize the pristine PVC cell. Additionally, we employ the same elements with a maximum size of $a/30$ to discretize the connectors of the resonators and a mesh size of $a/10$ for the remaining domains of the thick LRM unit cells.

In our numerical investigation, we assume surface wave propagation in the x-direction and impose periodic boundary conditions to the lateral edges of the unit cell in the same direction. To explore the dispersive features of the LRMs, we perform eigenfrequency analyses in the low-frequency range of $f = [0 - 10]$ kHz. During this analysis, we sweep the

wavenumber k within the range $k = [0, k_{max}]$, where $k_{max} = \pi/a$ represents the edge of the first Brillouin zone[4]. This approach allows us to effectively capture the numerical dispersion relations which are superimposed on the experimental and theoretical results in FIGs. 3(d-f) of the paper.

To better illustrate the numerical results, we present the real part of the normalized vertical displacements of the LRMs with 5 rows of resonators for the maximum wavenumber $k =$ 51.29 rad/m in FIGs. S4(b-d). For visualization purposes, we display the vertical wavefields by repeating the eigenmode of the column cell with a phase shift of $\exp(ikx)$ for 10 columns, which corresponds to a distance of $2\lambda_h$ along the surface wave propagation direction.

At the frequency ranges of the lower branch of the fundamental surface mode, resonators move in phase with respect to the host material, as illustrated in FIG. S4(b). At resonance ($f = f_r$), the surface waves are confined to the surface of the resonant layer. As the frequency increases beyond the resonance and upper edge of the bandgap, the resonators start to move out of phase, as shown in FIG. S4(d). This behavior is a characteristic feature of the dynamic interaction between the surface waves and resonators embedded within a hosting material. Moreover, the numerical solutions predict the existence of a plethora of flat modes within the bandgap (See FIG. 3(f) in the paper). These spurious modes are associated with the rotational motions of the local resonators as shown in FIG. S4(c). These numerical investigations contribute to better comprehending the dynamic response of the thick LRMs and their impact on surface wave propagation, further validating our theoretical analyses and experimental findings.

B. Harmonic analysis

To further explore the dispersive properties of the designed thick locally resonant layers, we developed a 3D numerical model of the metamaterial plate. In FIG. S5(a), the 2D schematic of the numerical model in the $x-z$ plane is depicted for the case of a resonant layer consisting of 5 rows of resonators. Harmonic analysis is conducted by applying a uniform unitary displacement ($u_x = 1$) at the location of the Piezo Actuator source on the experimental setup (refer to FIG. 2(a)). The static stability of the model during simulations is ensured by fixing the two bottom corners of the plate. Additionally, Low-Reflective Boundary (LRB) conditions are imposed on the lateral and bottom edges of the plate model to minimize the back-reflection of surface waves from the boundaries. A material damping of 5% is considered for the PVC material. The model is discretized with element size and dimensions matching those of the unit cell discussed in the previous section.

We perform frequency domain analysis within the frequency interval $f = [2000 - 10000]$ Hz. FIG. S5(b) demonstrates the displacement wavefield of the surface mode propagating along the free surface of the plate at the frequency of $f = 2500$ Hz. Furthermore, we analyzed all the flat modes within the bandgap, which are identified as surface modes by the criterion of Eq. (1). The numerical results in FIG. S5(c)exhibits a remarkable attenuation of surface waves after travelling 5 resonant cells (equivalent to a distance of λ_h) at a frequency inside the bandgap range ($f = 5820$ Hz). These findings provide additional confirmation that these flat modes are not genuine surface modes.

Finally, FIG. S5(d) displays the wavefield for the upper edge of the bandgap for the resonant layer with 5 rows of resonators at $f = 7017$ Hz. The upper edge of the bandgap represents the crossing point between the upper branch of the fundamental surface mode and the sound cone area where $c = C_{T,h}$. In the context of resonant metasurfaces, this point is referred to as the "conversion point," where surface modes are transformed into bulk shear waves[5,6]. Conversely, in the case of a thick resonant layer, this mode transforms into a leaky surface mode that disperses a portion of its elastic energy into the bulk of the plate[1].

The numerical results presented in this section prove the effectiveness of thick and finite-length LRMs in attenuating surface waves within the desired low-frequency range. These findings highlight the potential of LRMs as efficient structures for surface wave suppression, offering promising opportunities for practical applications that require the control and mitigation of surface wave propagation in various fields of engineering.

REFERENCES

[1] F. Zeighami, A. Palermo, and A. Marzani, "Rayleigh waves in locally resonant metamaterials," International Journal of Mechanical Sciences **195**, 106250 (2021).

[2] COMSOL Multiphysics®, "Comsol ab, stockholm, sweden." (2023).

[3] B. R. Mace and E. Manconi, "Modelling wave propagation in two-dimensional structures using finite element analysis," Journal of Sound and Vibration **318**, 884–902 (2008).

[4] L. Brillouin, *Wave propagation in periodic structure* (McGraw-Hill,, New York, NY, 1946).

[5] A. Palermo, S. Krödel, A. Marzani, and C. Daraio, "Engineered metabarrier as shield from seismic surface waves," Scientific Reports **6**, 39356 (2016).

[6] D. Colquitt, A. Colombi, R. Craster, P. Roux, and S. Guenneau, "Seismic metasurfaces: Sub-wavelength resonators and rayleigh wave interaction," Journal of the Mechanics and Physics of Solids **99**, 379–393 (2017).